

JOURNAL OF TECHNIQUES

Journal homepage: http://journal.mtu.edu.iq



RESEARCH ARTICLE - ENGINEERING (MISCELLANEOUS)

Enhancing Optimal Reactive Power Dispatch under Critical Contingencies Using MPC-GUPFC with FRT Capability and HPSOBAT Optimization

Sunday Adetona^{1*}, Adeola Balogun^{1*}, Frank Okafor¹

¹Department of Electrical & Electronics Engineering, University of Lagos, Lagos, Nigeria

* Corresponding author E-mail: sadetona@unilag.edu.ng

Abstract
This paper presents a unified and intelligent scheme for enhancing Optimal Reactive Power Dispatch (ORPD) under severe grid disturbances in the IEEE 30-bus system. A critical branch outage is first identified using a composite performance
index (PI) based on total power loss and total voltage variation. The most severe line removal introduces up to 10.0 MW of additional losses and a voltage deviation of 0.021 pu, significantly degrading system performance. To effectively counter this, a combined mitigation strategy is proposed, simultaneously applying a Fault Ride-Through (FRT) mechanism
and a Model Predictive Control based Generalized Unified Power Flow Controller (MPC-GUPFC). The MPC-GUPFC is dynamically controlled over a 5-step prediction horizon and optimally placed at sensitive bus triplets using a sensitivity-driven placement framework. The FRT capability ensures system stability during the disturbance, while the MPC-GUPFC
adaptively controls power flow and supports voltage during and after the faulty event. Quantitative results show that this coordinated FRT with MPC-GUPFC strategy reduces total power losses from 21.8 MW (post-outage without mitigation) to 12.2 MW, and worse-case voltage deviation from 0.136 pu to 0.060 pu, at a quantified MPC-GUPFC cost of \$55,226.15. Moreover, reactive power losses are minimized from 16.9 MVAr to 9.5 MVAr, and the system converges in fewer than 10 iterations, compared to over 20 iterations in the unmitigated case. The overall PI value is improved by over 43.79 %, demonstrating the superiority of the proposed approach in improving voltage stability, loss minimization, and post-contingency recovery.
e under the CC BY 4.0 license (http://creativecommons.org/licenses/by/4.0/) Publisher: Middle Technical University
_

Keywords: Optimal Reactive Power Dispatch (ORPD); GUPFC; FRT; Model Predictive Control (MPC); HPSOBAT.

1. Introduction

Modern electric power systems are increasingly challenged by rising electricity demand, growing penetration of renewables, and the imperative for operational resilience. Among the major operational concerns is the impact of critical contingencies, such as the sudden removal of a transmission line, which can result in severe voltage instability and increased power losses. Optimal Reactive Power Dispatch (ORPD) performs a pivotal function in sustaining system security along with minimizing these losses through coordinated control of generator voltages, reactive power injections, and transformer tap settings [1, 2]. The incorporation of Flexible AC Transmission System (FACTS) devices [3, 4], especially the Generalized Unified Power Flow Controller (GUPFC), has emerged as a promising solution due to its unique ability to simultaneously manage voltage, power flow, and reactive compensation across multiple transmission corridors.

Several recent studies have explored different approaches to improve power system performance under stressed conditions. For instance, [5] employed a hybrid Whale-BAT optimization algorithm for GUPFC-based ORPD in systems with high renewable energy penetration. Their results showed a 12% reduction in voltage deviation, although the study lacked a robust dynamic control framework during critical outages. Other researchers have turned to Model Predictive Control (MPC) to improve control of FACTS devices and renewable sources. Authors in [6] applied MPC strategies with superconducting magnetic energy storage to enhance the fault ride-through (FRT) effectiveness of wind energy systems. While their approach yielded notable improvements in post-fault voltage recovery, it did not consider ORPD integration or GUPFC coordination. Similarly, [7] demonstrated the use of MPC for low-voltage ride-through in inverter-based systems, achieving reduced active power deviations during voltage sags. However, this approach also did not incorporate GUPFC or address system-wide reactive power optimization under contingency scenarios.

In the context of ORPD optimization, [8] advanced a multi-objective hybrid algorithmic rule to reduce voltage deviations and power losses on the IEEE 30-bus system. Although effective under normal conditions, their method did not incorporate sensitivity-based GUPFC placement or examine fault-induced instability. Collectively, these studies reveal that despite various advancements, key gaps remain. Most notably, prior research has treated ORPD and FACTS-based dynamic control as isolated problems, rarely addressing them in a unified framework that incorporates fault ride-through strategies and predictive control. Additionally, no study to date has combined sensitivity-based placement of GUPFC with a coordinated MPC and FRT scheme under a critical line outage.

Nomenclature & Symbols									
ORPD	Optimal Reactive Power Dispatch	GUPFC	Generalized Unified Power Flow Controller						
PI	Performance Index	FACTS	Flexible AC Transmission System						
FRT	Fault Ride-Through	HPSOBAT	Hybrid Particle Swarm Bat Algorithm						
MM	MATLAB-MATPOWER	PQ bus	Load Bus						
TPL	Total Power Loss	PV bus	Generator Bus						
TVV	Total Voltage Variation	UPFC	Unified Power Flow Controller						
MPC	Model Predictive Control	EPG	Electric Power Grid						

The present study tackles these limitations by introducing a unique hybrid control framework that integrates MPC-based GUPFC control with FRT support into a contingency-aware ORPD model. A critical transmission line is first identified using a sensitivity-based performance index that evaluates the combined impact of power loss and voltage deviation. Thereafter, a GUPFC is injected at strategic PQ bus combinations to mitigate the adverse effects of the line outage. The device is controlled using MPC to dynamically manage reactive power flow and maintain system voltages, while also ensuring fault ride-through capabilities during transient disturbances. The hybrid particle swarm Bat (HPSOBAT) algorithmic rule is utilized to find solutions to the multi-objective ORPD problem with enhanced convergence and global search ability.

The remainder of the paper is coordinated as follows. Section 2 of the paper formulates the problems and methods for the identification of the critical outages in electrical power grid (EPG), optimal location and sizing GUPFC, and HPSOBAT based multi-objective ORPD optimization in the EPG without and with FRT-MPC based GUPFC. In section 3, the modeling and simulation analysis used in achieving the global goal of this study are exhibited and explained. The IEEE 30 bus-system used as an EPG is also exhibited and discussed in the section. Results obtained in the simulation environment to investigate the impact of critical contingencies without and with FRT and MPC based GUPFC on the ORPD in the EPG using HPSOBAT are presented and discussed in section 4. Lastly, Section 5 concludes with future research guidance.

2. Problem Formulation

The global target of this work is to examine the upshot of the critical contingencies on the ORPD in EPG without and with FRT and MPC based GUPFC. To achieve this goal, this section of the paper therefore presents the problem formulations for the identification of the critical outages in EPG, optimal location and sizing FRT-MPC based GUPFC, and HPSOBAT based multi-objective ORPD optimization in the EPG without and with FRT-MPC based GUPFC.

2.1. Problem formulation for the identification of the critical outages in EPG

Critical branches in an EPG are those whose failure would lead to a significant impact on the system, such as, increased active power losses, disruption in voltage stability, and excessive stress on remaining branches. Therefore, the core problem in this subsection of the paper is to evaluate the consequences of each branch outage, excluding the swing bus connections (branches 1 and 2), and rank them based on a composite performance index (PI).

2.1.1. Modeling of the EPG and base case power flow

The AC power balance equations [9-12] at every bus for each bus $i \in \aleph$ (set of all buses) are:

$$\begin{cases} P_i^g - P_i^d = V_i \sum_{j \in \mathbb{N}} V_j (G_{ij} cos \delta_{ij} + B_{ij} sin \delta_{ij}) \\ Q_i^g - Q_i^d = V_i \sum_{i \in \mathbb{N}} V_i (G_{ij} sin \delta_{ij} - B_{ij} cos \delta_{ij}) \end{cases}$$
(1)

In Eq. (1), the subscripts g and d stand for generation and demand respectively; P_i^d and Q_i^d are active and reactive power demand at bus i; P_i^g and Q_i^g active and reactive power generation at bus i; $V_i \angle \delta_i$ and $V_j \angle \delta_j$ are the voltage magnitudes and angles at buses i and j respectively; $Y_{ij} = G_{ij} + jB_{ij}$ is the (i, j) element of the bus admittance matrix and $\delta_{ij} = \delta_i - \delta_j$. Let the system state vector be denoted as x, and the bus-admittance matrix of the original system be represented by Y_{bus} ; hence, Eq. (1) can be compactly expressed as

$$f(x; Y_{bus}) = 0 (2)$$

where, the $x = [V \delta]^T [9-12]$; hence the base-case state can be denoted by

$$x^{(0)} = \left[V^{(0)} \delta^{(0)}\right]^T \tag{3}$$

The base case
$$x^{(0)}$$
 is obtained by solving $f(x^{(0)}; Y_{hus}) = 0$. (4)

where, $f(\cdot)$ denotes the set of power balance equations. The base-case per-bus voltage magnitudes are denoted by

$$V^{(0)} = \left[V_1^{(0)}, V_2^{(0)}, \dots, V_N^{(0)} \right]^T \tag{5}$$

And the base-case total power loss [9-12] be defined as

$$P_{loss}^{(0)} = \sum_{k \in \mathcal{L}} \left(P_{k,F}^{(0)} + P_{k,T}^{(0)} \right). \tag{6}$$

where, $P_{k,F}$ and $P_{k,T}$ are branch real power flows at the "From" and "To" ends respectively, and $\mathcal{L} = \{1, 2, \dots, \aleph_{br}\}$, set of branches, index $\ell \in \mathcal{L}$.

2.1.2. Outage modelling

For each nominee line $\ell \in \mathcal{L}_{cand} = \mathcal{L}_{cand} = \mathcal{L} \setminus \mathcal{E} = \{3,4,\cdots \aleph_{br}\}$, where the ejected lines are $\ell \in \mathcal{E} = \{1,2\}$, the outage is mimicked by setting its status to zero in the line data. The adapted admittance matrix is therefore $Y_{bus}^{(\ell)}$, and, if capable of being solved, the post-outage state is

$$x^{(\ell)} = \left[V^{(\ell)} \, \delta^{(\ell)} \right]^T \tag{7}$$

which must satisfy the power flow conditions

$$f(x^{(\ell)}; Y_{bus}^{(\ell)}) = 0.$$
 (8)

where, $x^{(\ell)}$ is the updated system state variables after the outage.

2.1.3. Impact metrics per outage *l*

The two impact metrics, total power loss increase (economic impact) and total voltage variation (technical/stability impact), are computed by juxtaposing $x^{(\ell)}$ and $x^{(0)}$. Let the total real power loss after outage ℓ be

$$P_{loss}^{(\ell)} = \sum_{k \in \mathcal{L}^{(\ell)}} \left(P_{k,F}^{(\ell)} + P_{k,T}^{(\ell)} \right). \tag{9}$$

where, $\mathcal{L}^{(\ell)}$ represents the group of lines after removing branch ℓ . The impact on total losses is therefore,

$$\Delta P_{loss}^{(\ell)} = P_{loss}^{(\ell)} - P_{loss}^{(0)} \tag{10}$$

The total voltage variation measures the degradation in voltage profile and contiguousness to stability limits. Let the post-outage per-bus voltage magnitudes be

$$V^{(\ell)} = \left[V_1^{(\ell)}, V_2^{(\ell)}, \cdots, V_N^{(\ell)} \right]^T \tag{11}$$

Then, the total voltage variation can be defined as

$$\Delta V_{dev}^{(\ell)} = \sum_{i \in \mathbf{R}} \left| V_i^{(\ell)} - V_i^{(0)} \right| \tag{12}$$

2.1.4. Composite performance index

To rank the severity of each outage ℓ , a scalar PI is formulated by combining the two metrics, Eq. (10) and Eq. (12), into a weighted sum:

$$PI^{(\ell)} = \omega_1 \Delta P_{loss}^{(\ell)} + \omega_2 \Delta V_{dev}^{(\ell)} \tag{13}$$

In Eq. (13), ω_1 and ω_2 are economic weight coefficient (priority on minimizing power losses) and technical weight coefficient (priority on voltage stability) respectively; they are subject to $\omega_1 + \omega_2 = 1$. In assigning weight coefficients to ensure both metrics are dimensionally balanced, we set $\omega_1 = 0.7$ (since reducing losses has a strong economic impact), $\omega_2 = 0.3$ (as voltage stability is critical but secondary to economic efficiency). If the post-outage power flow does not converge, set $PI^{(\ell)}$ to+ ∞ .

2.1.5. Optimization problem

The vital line ℓ^* is identified as the one that maximizes the $PI^{(\ell)}$

$$\ell^* = arg \max_{\ell \in \mathcal{L}_{cand}} PI^{(\ell)} \tag{14}$$

This branch is deemed the most critical because its outage leads to the largest combined economic and technical violation according to the defined criteria. Eq. (14) is subject to following constraints, the post-outage system state $x^{(\ell)}$ that must satisfy Eq. (4), and generator and branch operational limits that must be enforced during the power flow. In this study, if a valid solution cannot be found, this is indicated by setting $PI^{(\ell)} = \infty$.

2.2. Problem formulation for the optimal location of the MPC based GUPFC

The GUPFC is a FACTS device designed to optimize voltage profiles, reduce transmission losses, and improve power system stability. It is a more versatile and integrated version of the UPFC and is particularly effective for multi-line and multi-bus power flow regulation [13, 14]. The model of GUPFC is presented in Fig. 1 that reveals that a common structure of GUPFC includes one shunt converter at the sending bus, two or more series converters injected into adjacent lines [15-17], and a common dc link connecting all converters. The core objective is to find the most effective location for a GUPFC to enhance overall system performance.

It should be stated here that controlling the GUPFC effectively is critical for achieving its multi-functional roles. To that effect, Table 1 presents several control strategies that have been developed in the literature [18-24] to manage GUPFC behaviours.

2.2.1. State variables and network equations

The AC power balance equations at every bus for each bus $i \in \aleph$, base-case per-bus voltage magnitudes, and base-case total power loss are as defined in Eq. (1), Eq. (5), and Eq. (6) in section 2.1.1 respectively.

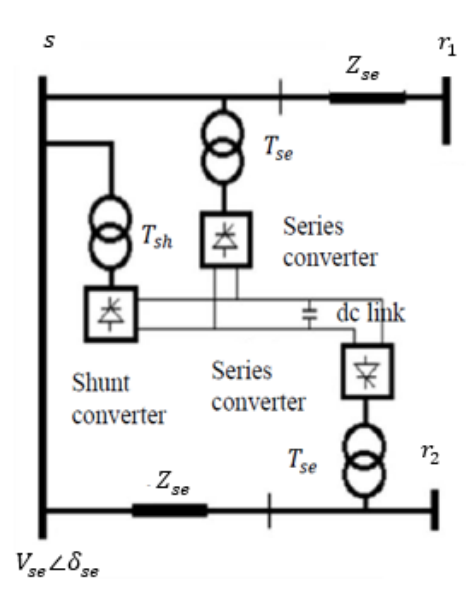


Fig. 1. The model of GUPFC

Table 1. Control methods for GUPFC

Control method	Main features	Suitable for		
PI Control	Simple, easy to implement	Basic regulation tasks		
Model Predictive	Predictive, multi-variable optimization	Dynamic operation, congestion management		
Fuzzy Logic	Rule-based, adaptive, nonlinear	Uncertain systems, heuristic adaptation		
Sliding Mode	Robust, fast, nonlinear	Systems with high disturbances		
Neural Networks	Learning-based, intelligent control	Pattern recognition, nonlinear compensation		
GA/Metaheuristics	Global optimization, parameter tuning	Placement, tuning of control parameters		

2.2.2. GUPFC equivalent modelling in the formulation

In this study, we determine the optimal location for an MPC based GUPFC in an EPG by selecting the best triplet of buses (s, r_1, r_2) , where s is the sending bus, and r_1 and r_2 are receiving buses. For a nominee combination $c = (s, r_1, r_2)$, the script we developed models the GUPFC by inserting (or modifying) series branches between the sending bus and each receiving bus. In the study, set of PQ buses are only considered for the injections of GUPFC $(PQ \subset \aleph)$, and, all buses connected to tap-changing transformers are excluded from GUPFC receivers $(\{r_1, r_2\} \subseteq \aleph \setminus T)$; therefore,

$$|c| = {|\mathcal{V}| \choose 3}, where \, \mathcal{V} \setminus \mathcal{T}.$$
 (15)

The equivalent branch parameters used in our script are constant values:

$$Z_{se} = R_{se} + jX_{se}, \quad V_{se} \tag{16}$$

With reference to circuit theory, each modified/added branch k between s and r_i has series impedance Z_{se} and an equivalent series voltage injection V_{se} . These values are used to either modify an existing branch or append a new branch to Y_{bus} . Therefore, mathematically, the post-GUPFC admittance matrix is represented by $Y_{bus}^{(c)}$.

2.2.3. Post-injection power flow and feasibility

For each nominee c, solve the modified power flow

$$f(x^{(c)}; Y_{bus}^{(c)}) = 0 (17)$$

where, $x^{(c)}$ is the updated system state variables after the outage.

Eq. (17) is subject to generator and branch operational limits:

$$\begin{cases} P_i^{g,min} \leq P_i^g \leq P_i^{g,max}, \forall i \in g \\ Q_i^{g,min} \leq Q_i^g \leq Q_i^{g,max}, \ \forall i \in g \\ |S_k| \leq S_k^{max}, \forall k \in \mathcal{L} \cup \mathcal{L}^{(c)} \end{cases}$$

$$(18)$$

If the power flow for combination c is infeasible, then the $PI^{(c)} = \infty$.

2.2.4. Performance index

Let the total real and reactive power losses [9-12] be

$$P_{loss} = \sum_{i \in g} P_i^g - \sum_{i \in N} P_i^d, \ Q_{loss} = \sum_{i \in g} Q_i^g - \sum_{i \in N} Q_i^d. \tag{19}$$

Hence, the power loss component is

$$S_{loss} = P_{loss} + jQ_{loss}. (20)$$

And, the voltage deviation component

$$\Delta V_{dev} = \sum_{i \in \mathbf{N}} |V_i - 1.0| \tag{21}$$

A scalar PI is formulated by combining the two metrics into a weighted sum

$$PI^{(c)} = \omega_3 S_{loss} + \omega_4 \Delta V_{dev} \tag{22}$$

2.2.5. Sensitivity (optimization) statement

The sensitivity analysis seeks the combination c^* that minimizes $PI^{(c)}$,

$$c^* = \arg\min_{c \in C} PI^{(c)} \tag{23}$$

where, C denotes group of nominee 3-bus combinations c. Eq. (23) is subject to the network equations and operational limits:

$$\begin{cases} f(x^{(c)}; Y_{bus}^{(c)}) = 0\\ P_i^{g,min} \le P_i^g \le P_i^{g,max}, Q_i^{g,min} \le Q_i^g \le Q_i^{g,max}\\ |S_k| \le S_k^{max}, \forall i \in g, \forall k \in \mathcal{L} \cup \mathcal{L}^{(c)} \end{cases}$$

$$(24)$$

In implementation, the algorithm is a brute-force enumeration; evaluate for every then pick the giving the minimum finite If any run is infeasible that receives and is effectively discarded. Eq. (23) is subject to Eq. (17) through Eq. (22) for each nominee triplet.

2.3. Problem formulation for the HPSOBAT based multi-objective ORPD in EPG

The global goal of this study is to perform ORPD under different grid scenarios using a multi-objective metaheuristic algorithm, HPSOBAT. The three grid schemes $s \in \{0,1,2\}$ considered are baseline ORPD (s = 0), outage scenario (s = 1), and outage + Fault Ride Through (FRT) + Model Predictive Control (MPC) based GUPFC scenario (s = 1).

2.3.1. State variables and network equations under different scenarios

For each bus $i \in \aleph$ under scenario s, the power balance equations are:

$$\begin{cases}
P_i^{g(s)} - P_i^d = V_i^{(s)} \sum_{j \in \mathbb{N}} V_j^{(s)} \left(G_{ij}^{(s)} cos \delta_{ij}^{(s)} + B_{ij} sin \delta_{ij}^{(s)} \right) \\
Q_i^{g(s)} - Q_i^d = V_i^{(s)} \sum_{j \in \mathbb{N}} V_j^{(s)} \left(G_{ij}^{(s)} sin \delta_{ij}^{(s)} - B_{ij} cos \delta_{ij}^{(s)} \right)
\end{cases}$$
(25)

with $\delta_{ij}^{(s)} = \delta_i^{(s)} - \delta_j^{(s)}$ and $Y_{ij}^{(s)} = G_{ij}^{(s)} + jB_{ij}^{(s)}$. Eq. (25) can be compactly expressed as

$$f\left(x^{(s)}; Y_{bus}^{(s)}\right) = 0 \tag{26}$$

Eq. (26) is subject to the following constraints

$$\begin{cases} V_{i}^{g,min} \leq V_{i}^{g} \leq V_{i}^{g,max}, i \in g \\ Q_{i}^{g,min} \leq Q_{i}^{g} \leq Q_{i}^{g,max}, i \in g \\ \mathfrak{t}_{k}^{min} \leq \mathfrak{t}_{k} \leq \mathfrak{t}_{k}^{max}, k \in \mathcal{T} \end{cases}$$

$$(27)$$

2.3.2. Decision and Optimization variables for the ORPD

Represent the decision vector for ORPD, which incorporates all the variables optimized by the HPSOBAT procedure by

$$x_{opt} = [V^g Q^g t]^T \tag{28}$$

where, $V^g = \begin{bmatrix} V_i^g \end{bmatrix}_{i \in g'}$, $Q^g = \begin{bmatrix} Q_i^g \end{bmatrix}_{i \in g'}$ and $\mathfrak{t} = [\mathfrak{t}_k]_{k \in T}$ are setpoints of generator voltages, generator reactive powers, and tap settings of transformers respectively.

2.3.3. Decision and Optimization variables for the ORPD

At each ORPD iteration the algorithm evaluates a scalar objective combining real power loss and voltage deviation:

$$J(x_{opt};s) = \omega_1 P_{loss}^{(s)}(x_{opt}) + \omega_2 \Delta V_{dep}^{(s)}(x_{opt})$$

$$\tag{29}$$

where,
$$P_{loss}^{(s)} = \sum_{k \in \mathcal{L}} \left(P_{k,F}^{(s)} + P_{k,T}^{(s)} \right)$$
. (30)

where, $P_{k,F}$ and $P_{k,T}$ are branch real power flows at the "From" and "To" ends respectively. And voltage profile deviation is defined as

$$\Delta V_{dev}^{(s)} = \sum_{i \in \mathbb{N}} \left| V_i^{(s)} - 1.0 \right| \tag{31}$$

In a situation where a power-flow iteration fails to converge, the objective is penalized, $J(\cdot) = M_{penality}, M_{penality} \gg 1$. And for each s, the algorithm seeks:

$$x_{opt}^{(s)*} = \arg\min_{x_{opt}} J(x_{opt}; s)$$
(32)

Eq. (32) is subject to $f\left(x^{(s)}; Y_{bus}^{(s)}\right) = 0$; operational limits on V^g , Q^g , t; and $\left|S_k^{(s)}\right| \leq S_k^{max}$, $\forall k \in \mathcal{L}^{(s)}$. The $Y_{bus}^{(s)}$ may bank on \mathfrak{t} , and, on added elements from GUPFC for the s. The HPSOBAT metaheuristic carries out the exploration, and brings forth a progression of intermediate solutions $\left\{J_n^{(s)}\right\}_{n=1}^{\infty}$.

2.3.4. Modeling of scenario with FRT and MPC on GUPFC

In the outage scenario (s = 1), a branch outage in between buses a and b is imitated by taking away its accompanying line from its group of branches, and compute again its Y_{bus} .

$$Y_{bus}^{(1)} = Y_{bus}^{(0)} - Y_{ab} E_{ab} \tag{33}$$

This is analogously enforced by removing the row(column) share of that line from the system data architecture. In Eq. (33), $Y_{bus}^{(0)}$ is the original Y_{bus} , whereas, E_{ab} is an incidence matrix that denotes the effect of deleting(modifying) a branch in between buses a and b in the Y_{bus} . The function of E_{ab} is to correct the Y_{bus} when Y_{ab} is taken out or modified; and it is mostly zeros with +1 and -1 at the positions corresponding to buses a and b.

Scenario 2 (s=2) involves introduction of both FRT adjustments and Model Predictive Control (MPC) mechanisms. For the FRT adjustments ($s=2_1$) scheme, we developed a model (like that in [25]) that mimics FRT behaviour that adjusts voltages and demands during a short disturbance period. For each faulted bus i, the voltage $V_i(t)$ is reduced by $\delta_v(t)$ to imitate the impact of the fault \mathcal{F} . Nevertheless, it is prevented from falling below V_{min} , and as such, it behaves as a lower limit. Also, the active power demand P_i^d is cut down by a factor $\gamma(t)$ to imitate the momentary load drop. The above scenario is mathematically expressed as

$$\forall i \in \mathcal{F}: \ V_i(t) \leftarrow \max(V_i(t) - \delta_v(t), V_{min}), P_i^d(t) \leftarrow P_i^d(1 - \gamma(t)), \forall t \in [t_f, t_c + \Delta t], \ i \in \mathfrak{B}_{critical}$$
 (34)

In the equation, t_f , t_c , Δt , and $\mathfrak{B}_{critical}$ are time of fault, time of fault clearing, short post-fault recovery window, set of critical buses (load and GUPFC-connected) monitored for FRT, and voltage at bus i during dynamic simulation respectively.

GUPFC with MPC ($s = 2_2$): The GUPFC is imitated by injecting equivalent branch elements and a controllable Q injection. The MPC works out a progression of Q setpoints over a prediction horizon H to trail a mark reactive power Q_{target} and to minimize predicted voltage deviation [26]. In real-time the H is taken not to exceed 2 to avoid computational burden on the processors used in determining the switching of the power electronics semiconductors in the converters of the GUPFC. Selecting H = 1 is very common because of its simplicity and reduced computational cost. A higher performance digital signal processor (DSP) will be required for hardware implementation when selecting H = 2. Then a per-step MPC problem is solved viz: The state equations (model) obtained at the outputs of the converters of the GUPFC are discretized via forward Euler's method. Then given current state z_0 , discover control sequence $u = [u_0, \dots, u_{H-1}]$ that minimizes Eq. (35) is discovered at every stage.

$$\min_{\mathbf{k}} \sum_{k=0}^{H-1} \ell(z_k(u), u_k) \text{ subject to } u_{min} \le u_k \le u_{max}$$
 (35)

where, \mathbb{k} represents discrete time step index within the H, and a sample stage cost function (like [26]) that is minimized at every stage is given in Eq. (36).

$$\ell(z, u) = \|V(z) - V_{ref}\|_{2}^{2} + \rho(u - Q_{target})^{2}. \tag{36}$$

In Eq. (36), z denotes system state, u represents control input sequence over the H, each u_k is a Q setpoint. Also, V_{ref} is the target voltage, V(z) represents predicted V_i under z, Q_{target} represents target Q injection, $(u - Q_{target})^2$ stands for penalty for deviating from Q_{target} , ρ denotes weighted factor balancing importance of voltage regulation against Q tracking. Only the first computed control action u_0 is enforced (receding-horizon conceptualization), the GUPFC then alters $Y_{hus}^{(2)}$ by adding branch rows imitating the series(shunt) identical:

$$Y_{bus}^{(2)} \leftarrow Y_{bus}^{(2)} + \Delta Y_{GUPFC}(u_0) \tag{37}$$

where, $Y_{bus}^{(2)}$ is updated Y_{bus} utilized for power flow with series compensation, $\Delta Y_{GUPFC}(u_0)$ is the admittance upset injected by the GUPFC at initial control u_0 .

2.3.5. Model for Cost of MPC based GUPFC

It evaluated the operational cost (per MPC step \mathbbm{k}) of the MPC based GUPFC mechanism by using the model in [27] that is defined as $C_{GUPFC,\mathbbm{k}}(S_{GUPFC,\mathbbm{k}}) = 0.0003S_{GUPFC,\mathbbm{k}}^2 - 0.2691S_{GUPFC,\mathbbm{k}} + 188.22 - GUPFC cost function (\$/kVar)$ (38)

In Eq. (38), $C_{GUPFC,k}$ is measured in \$/kVar, and $S_{GUPFC,k}$ (kVar) is known as the GUPFC effective loading [27]. In this study, the $S_{GUPFC,k}$ is obtained from simulation after s = 2.

$$S_{GUPFC,k} \approx |Q_{2,k} - Q_{1,k}| \tag{39}$$

where, $Q_{1,k}$ and $Q_{2,k}$ denote the Q that flow on the two controlled routes after their positioning.

2.3.6. HPSOBAT

The HPSOBAT algorithm involves hybridization of PSO and Bat (BAT) algorithms, with the aim of exploiting the exploration capability of PSO and the local searching ability of the BAT to efficiently solve the ORPD problem. The conceptualization of the HPSOBAT [28, 29] used in the ORPD problem in this study is presented in Eq. (40) through Eq. (44).

$$v_{id}^{t+1} = \alpha \left(\omega_{id}^{t} + c_1 r_1 \cdot (pbest_{id} - x_{id}^{t}) + + c_2 r_2 \cdot (gbest_{gd} - x_{id}^{t}) \right)$$
(40)

$$x_i^{t+1} = (1-r).x_i^t + r.pbest_i + v_i^{t+1}$$
(41)

In Eq. (40) and Eq. (41), v_{id}^{t+1} is the velocity of particle (bat) i for iteration t+1 in a d-dimentional search space, x_{id}^{t} is the position of particle (bat) i for iteration t in a d-dimentional search space, x_{i}^{t+1} is the position of particle (bat) i at time t+1 in a d-dimentional search space, ω is the inertia weight, c_1 and c_2 are the cognitive and social coefficients, r_1 and r_2 are random values in [0, 1], $pbest_i$ is the best position of particle (bat) i in a d-dimentional search space, $gbest_g$ is the global best position across all particles (bats) in a d-dimentional search space, ω is the inertia weight, and r is the pulse rate. In Eq. (40), according to [28, 29] ω is defined as

$$\alpha = (\mathfrak{C}/r)f_i \tag{42}$$

In Eq. (42), \mathfrak{C}/r is the average loudness of all the bats at iteration t, and f_i is the frequency that directs or determines the rate of the movement of bat i for iteration t in a d – dimentional search space, and it is defined as

$$f_i = f_{min} + (f_{max} - f_{min})\beta, \ \beta \in [0,1].$$
 (43)

where, f_{min} and f_{max} are minimum and maximum allowable frequencies for all bats; and are assigned the values of 0 and 100 Hz respectively, as stipulated in [27].

$$\omega = \omega_{min} + \left(\omega_{max} - \left(\frac{\omega_{max} - \omega_{min}}{t_{max}}\right)\right)r \tag{44}$$

In Eq. (44), ω_{min} and ω_{max} are the minimum and maximum allowable inertial weight for the bat i, and are assigned the values of 0.4 and 0.9 respectively, as stipulated in [30, 31].

3. Modeling and Simulation Analysis

To investigate the impact of critical contingencies without and with FRT and MPC based GUPFC on the ORPD in the EPG, the problems that were formulated in section 2 of this paper were modeled and simulated in the MATLAB [32] - MATPOWER [33] environment. To that effect, this section of the paper presents and discusses the flowchart diagrams that were developed to realize various MATLAB-MATPOWER (MM) scripts and functions used in achieving the global goal of this study. The IEEE 30 bus-system was used as an EPG. This testbed is also presented and discussed in this section.

3.1. Testbed for the investigation

A single line diagram of the testbed used in studying the impact of critical contingencies on the EPG without and with MPC-GUPFC and FRT mechanisms on the ORPD in the MM simulation environment is presented in Fig. 2.

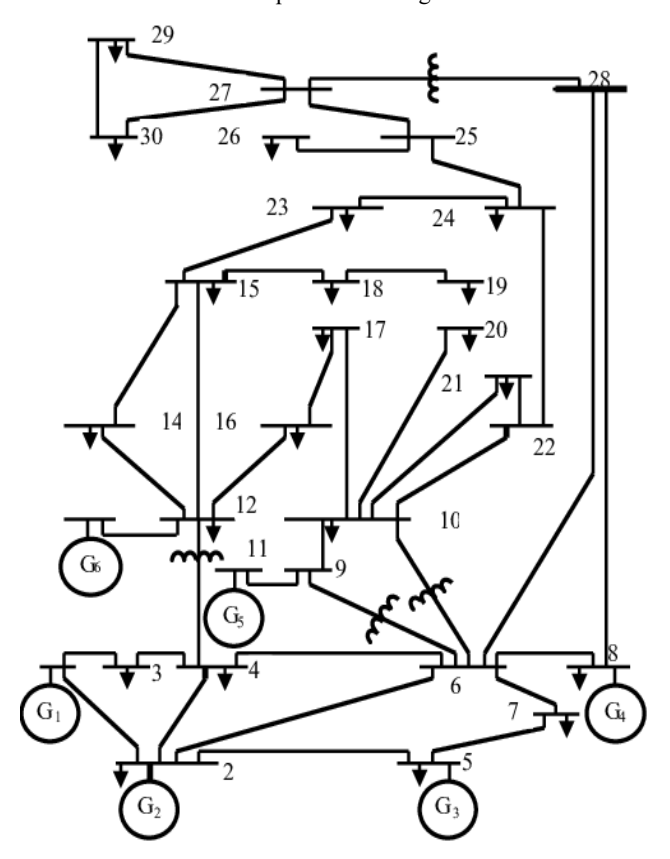


Fig. 2. One line diagram of the IEEE 30-bus system [34]

Fig. 2 reveals that the testbed has 6 generating units that are available at buses 1 (used as a swing bus in this study), 2, 5, 8, 11 and 13; it has 4 regulating transformers that are inserted in between buses 6-9, 6-10, 4-12 and 27-28; and a total number of 41 transmission lines. The line and bus data of the testbed are available in [34]. In this study, voltage limits for PV and PQ buses, and transformer tap settings are assumed to be 0.90 pu-1.10 pu, 0.95 pu-1.05 pu, and 0.95 pu-1.05 pu respectively.

3.2.1. Model for pinpointing severe outages in EPG

Fig. 3 presents the flowchart employed to carry out the MM script for pinpointing the critical branch(es) on EPG; and hence investigating the impact of the severe exigency situations on the EPG without and with FRT and MPC-GUPFC on the ORPD.

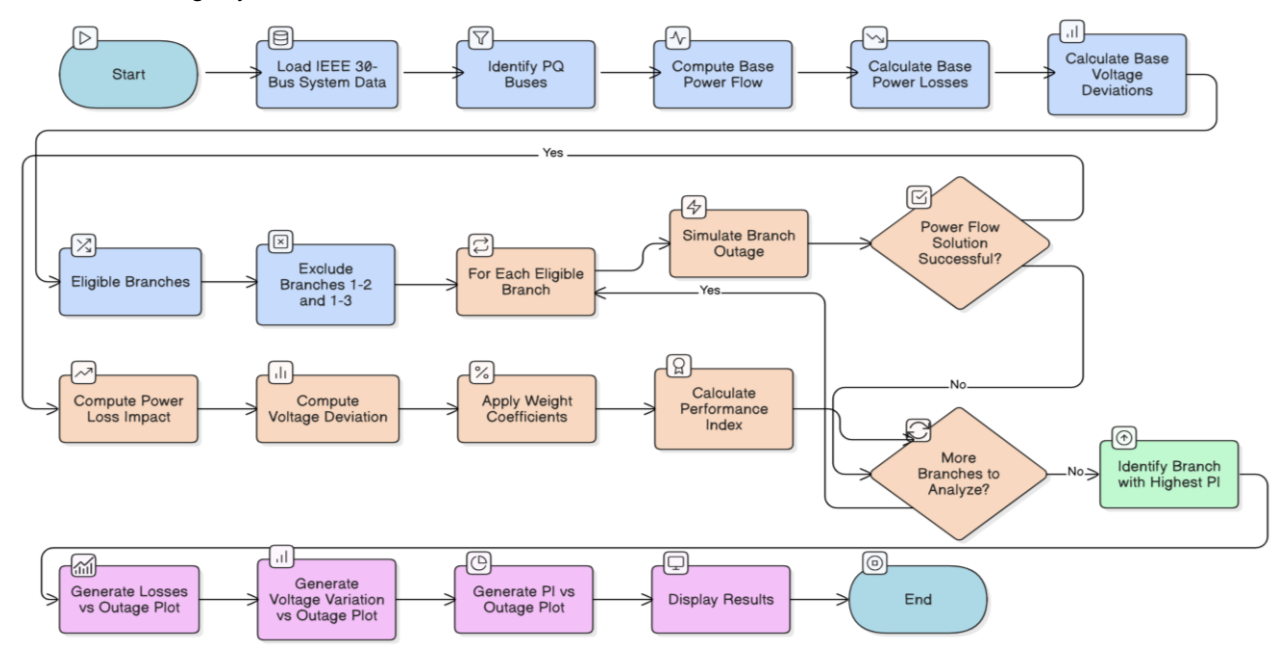


Fig. 3. The flowchart for the execution of the script for identification critical line outage of the EPG in the MATLAB environment

Subsection 2.1 of this paper provided the ideas used to accomplish Fig. 3. The contingency analysis process was initiated by loading the IEEE 30-bus system data into the computational environment. Following initialization, all potential PQ buses were identified, as these serve as the primary candidates for voltage and reactive power variations. A base power flow was then performed to establish the reference operating point of the system, providing baseline values for active power losses and bus voltage deviations. These baseline metrics served as benchmarks for assessing the impact of each contingency scenario. Subsequently, eligible branches for contingency analysis were determined. Certain branches, such as lines 1-2 and 1-3, were excluded due to their critical nature and predefined operational constraints. Each remaining branch was then subjected to a single-line outage simulation. In cases where the outage resulted in non-convergence of the power flow solution, the scenario was discarded, and the algorithm proceeded to the next branch. For each successfully simulated outage, two primary performance indicators were computed. The first was the power loss impact, which quantifies the change in total system active power losses relative to the baseline case. The second was the voltage deviation, which measures the extent of voltage fluctuations across all buses. To ensure balanced assessment, these indicators were combined through a weighted formulation, where predefined coefficients reflected their relative importance. The performance index (PI) was then derived as a weighted sum of the power loss impact and voltage deviation. This procedure was iteratively repeated across all eligible contingencies. At the conclusion of the analysis, the branch outage associated with the maximum PI value was identified as the most critical contingency in the network. The results were then processed to generate graphical outputs, including plots of losses versus outage, voltage deviations versus outage, and PI versus outage. These visualizations provided a comprehensive view of system vulnerability under different contingency conditions. Finally, the outcomes were consolidated into a single framework to support decisionmaking. The identification of critical contingencies, alongside their quantified impacts, offered valuable insights for reinforcement strategies and optimization schemes actions in this study.

3.2.2. Model for the optimal location of the MPC-GUPFC

Fig. 4 presents the flowchart employed in this study to carry out the MM script for identifying the most desirable possible location of the MPC-GUPFC on EPG. Subsection 2.2 of this paper provided the ideas used to accomplish Fig. 4. With reference to the figure, the IEEE 30-bus test system was first loaded into the simulation environment, and PQ buses were identified as candidate locations for MPC-GUPFC placement. Buses associated with tap-changing transformers were excluded, and all valid three-bus combinations were generated. A baseline operating case was then established by performing a power flow on the original network, from which a performance index (PI) was computed to represent the system's operating condition. This baseline PI served as the benchmark for evaluating improvements. Each candidate placement was subsequently assessed through an iterative sensitivity analysis. For every bus combination, the GUPFC was inserted, power flow analysis was carried out, and a new PI was computed. The results were compared against the best case recorded, and updates were made whenever improvements were observed. After all combinations were tested, the configuration yielding the optimal PI was identified. To aid interpretation, all PI values were visualized in a comparative bar chart, with the optimal placement highlighted. This systematic approach ensured a rigorous and transparent determination of the best MPC-GUPFC location in the IEEE 30-bus system.

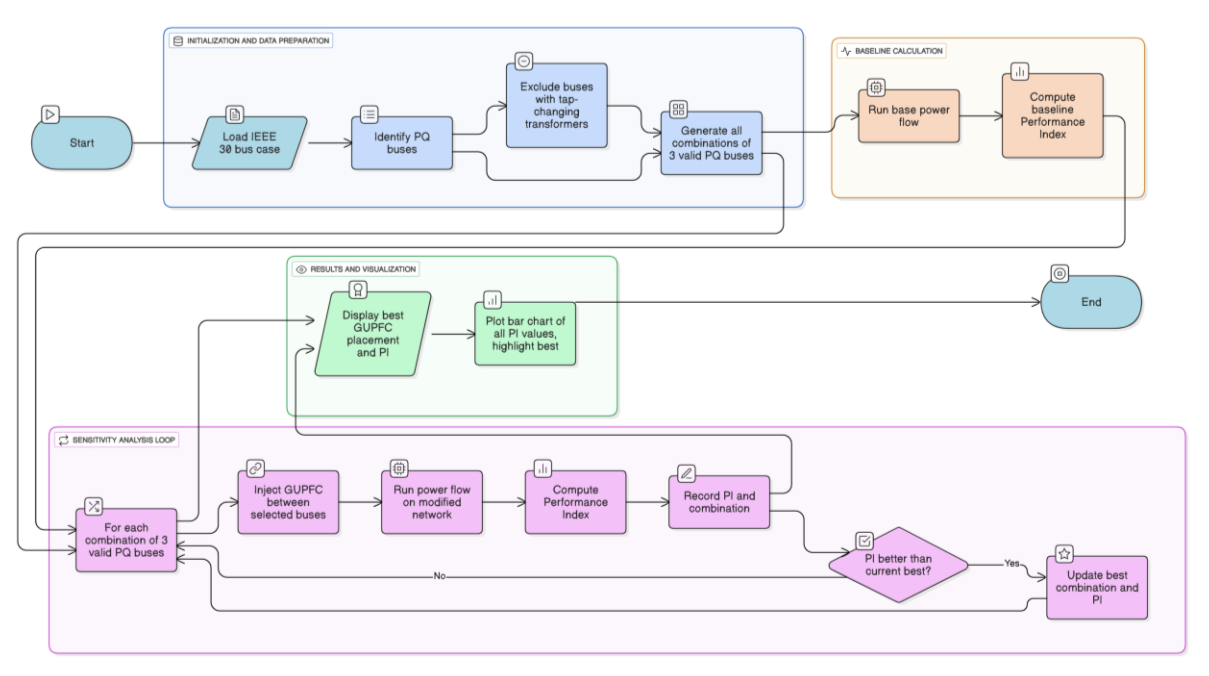


Fig. 4. The flowchart for the execution of the script for the optimal location of the MPC based GUPFC in the EPG in the MATLAB environment

3.2.3. Model for the HPSOBAT based multi-objective ORPD in EPG

Fig. 5 presents the flowchart employed in the development of the MM script used for investigating the conditions of the testbed before, during and after severe contingencies on the EPG without and with FRT and MPC-GUPFC on the ORPD.

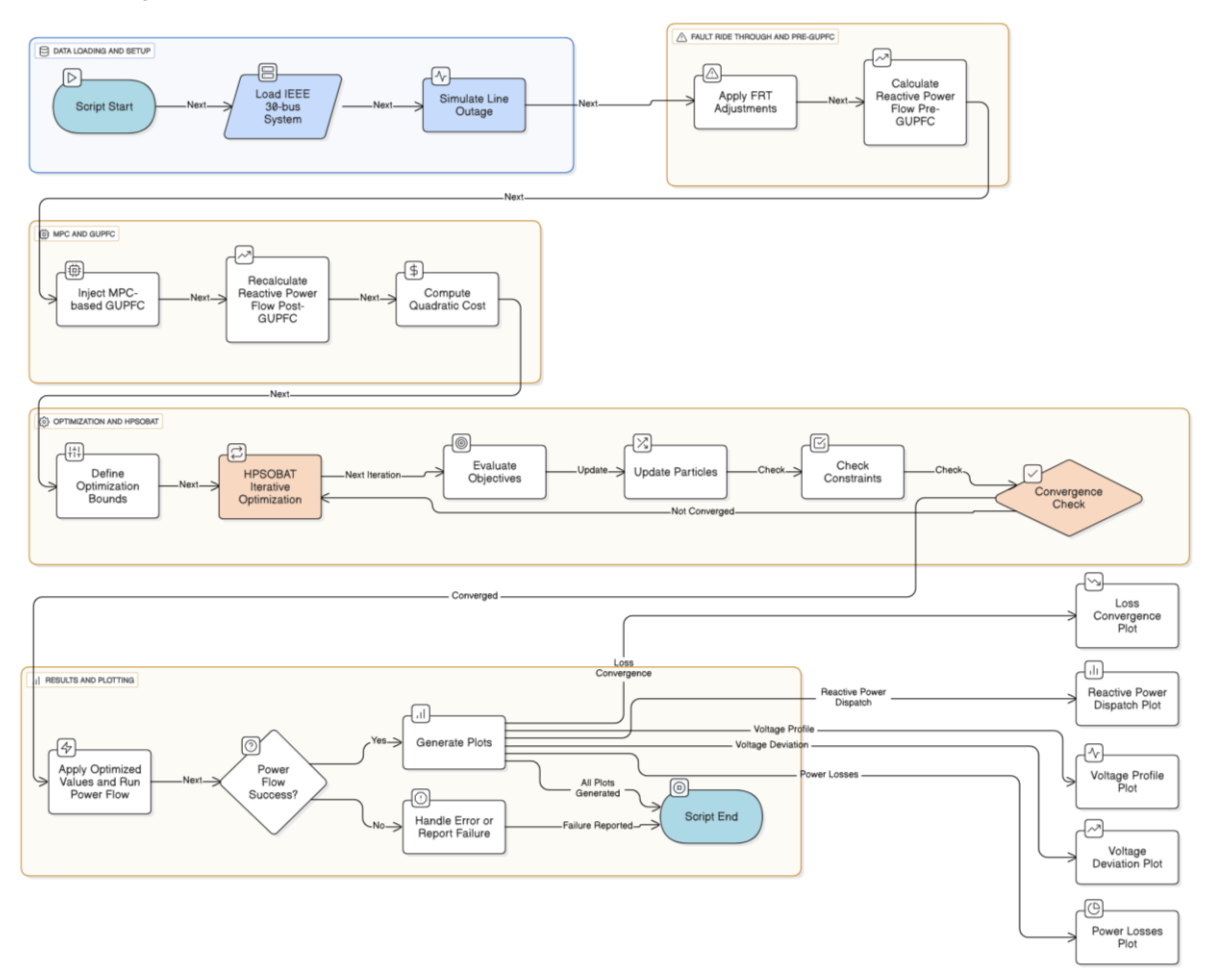


Fig. 5. The flowchart for the execution of the script for the HPSOBAT based multi-objective ORPD in EPG in the MATLAB environment

The procedure was initiated by loading the IEEE 30-bus system into the simulation environment, after which transmission line outages were simulated to represent contingency conditions. To ensure system resilience, Fault Ride-Through (FRT) requirements were applied, and the reactive power thresholds for GUPFC operation were calculated. This established the baseline against which the performance of the MPCbased GUPFC was assessed. In the next stage, the MPC-based GUPFC model was incorporated into the network. The device was reconfigured to regulate reactive power flow according to predicted system states, and the associated installation cost was computed. This enabled the assessment of both technical and economic impacts of GUPFC placement. The optimization stage was then carried out using the HPSO-BAT. Decision variable bounds were first defined, and the objectives were evaluated iteratively. Particles were updated according to the optimization rules, and system constraints, including voltage limits and reactive power bounds, were checked in each iteration. A convergence check was performed, and the loop was repeated until the stopping criterion was satisfied, at which point the global optimum solution was obtained. Upon convergence, the optimized power flow incorporating the MPC-based GUPFC was applied to the system. The performance of the solution was verified against system objectives. In cases where success was achieved, results were passed to the analysis stage; otherwise, error handling and failure reporting mechanisms were invoked. The validated results were then used to generate comparative plots, which included voltage profiles, reactive power dispatch, and total power losses before and after MPC-GUPFC integration. Finally, the results obtained were consolidated for interpretation. The optimized reactive power dispatch, improved voltage stability profile, and minimized transmission losses were presented as key outcomes of the methodology. By combining contingency simulation, MPC-based GUPFC modeling, advanced optimization, and result visualization, a rigorous framework for optimal reactive power dispatch in the IEEE 30-bus system was established.

4. Results and Discussion

4.1. Simulation results and discussion

4.1.1. Simulation results for studying the critical branch outages in EPG

Fig. 6 presents the simulation results of critical branch outage analysis for the testbed. It evaluates how line outages impact the system in terms of Total Power Loss (TPL), Total Voltage Variation (TVV), and Performance Index (PI). Each subplot represents these metrics across branch numbers excluding swing bus lines.

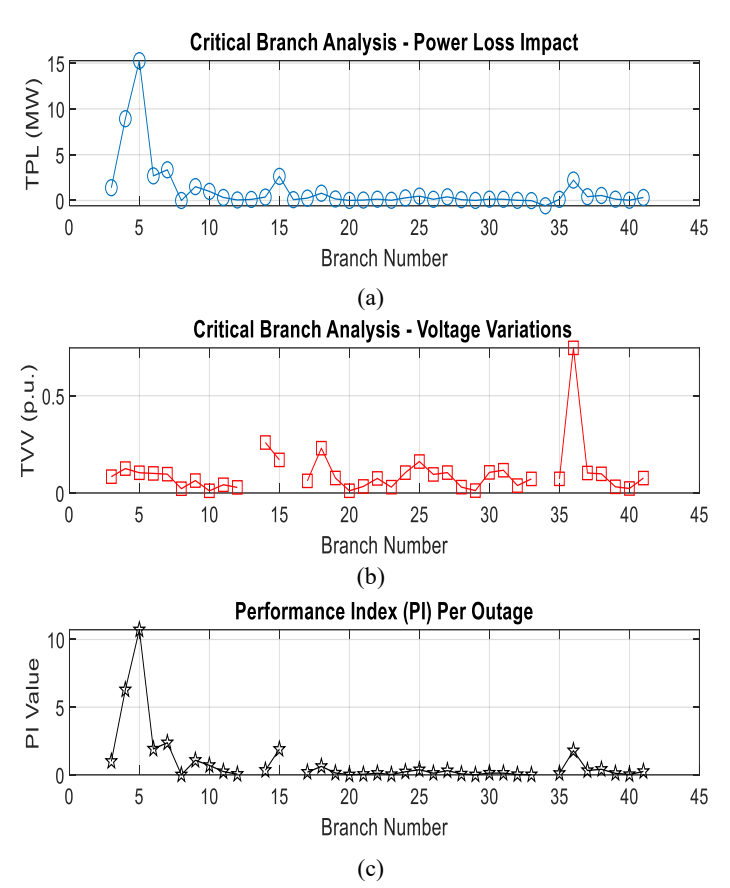


Fig. 6. The simulation results of the critical contingency analysis on the testbed

Fig. 6(a) is a plot of TPL against branch number. It is evident from the plot that branch 5 causes the highest increase in power loss (~15 MW) when taken out of service, and most other branches cause minimal increases in power loss (~1–3 MW). This shows that branch 5 is critical for system efficiency. Its outage severely disrupts power flow and increases system losses, and branches with low TPL impact are less critical from an economic loss perspective. Fig. 6(b), TVV versus branch number, reveals that branch 36 shows an abrupt voltage deviation, indicating a possible localized instability, whereas, other branches show varying levels of voltage variation, mostly within 0 - 0.25 pu. This indicates that outage of branch number 36 is likely to disrupt voltage regulation significantly at affected buses. This suggests technical vulnerability, possibly due to limited local voltage support or high impedance paths. Fig. 6(c) is the plot of PI against branch number. The highest PI value occurs at branch 5, indicating it is the most critical line when considering both economic and technical criteria. A smaller secondary peak occurs near

branch 36, due to its high voltage deviation. The PI formulation combines both economic cost (TPL) and technical stability (TVV), therefore, branch 5 is the most critical line overall, followed by branch 36 from a voltage sensitivity perspective. These results identify the most critical branches in the network based on multi-criteria evaluation.

4.1.2. Simulation results for studying the optimal location of the MPC based GUPFC

Fig. 7 presents the outcome of a comprehensive sensitivity analysis conducted to determine the optimal placement of an MPC-GUPFC in the IEEE 30-bus system. The analysis considers various combinations of one sending bus and two receiving buses and evaluates the system's response in terms of a performance index (PI), which is a composite metric used to evaluate the effectiveness of each placement configuration. Due to visual clarity constraints, only selected combinations are labelled. The PI-axis shows the computed PI for each combination, with lower values indicating more effective placements.

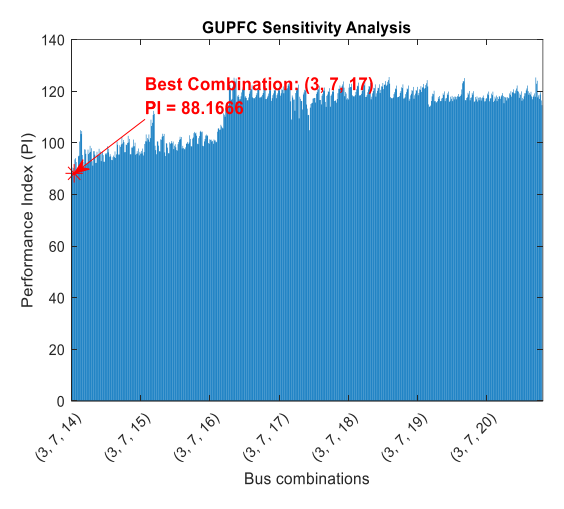


Fig. 7. The MPC-GUPFC sensitivity analysis across bus combinations

From the plot, the optimal configuration was identified as: Sending bus: 3, receiving buses: 7 and 17, and Minimum PI: 88.1666. This configuration is highlighted in red on the plot with a star marker and accompanying annotation. It represents the most effective placement for the MPC-GUPFC in terms of minimizing both system losses and voltage deviation. This result underscores the critical influence of placement strategy on the effectiveness of MPC-GUPFC devices in enhancing system performance. It also justifies the use of predictive control mechanisms and systematic sensitivity analysis in FACTS device allocation.

4.1.3. Simulation results for studying the behaviour of ORPD on the EPG under different scenarios

Fig. 8 presents a convergence plot that compares total power loss across three different scenarios in an iterative optimization or control simulation, over 100 iterations. The red curve is scenario v0 - loss history, which is the base (normal operating) case. It is evident from the plot that the initial loss is ≈ 12.2 MW, which converges quickly to around 11.8 units, represents the lowest loss scenario of all. The blue curve is an outage - loss history that represents system behaviour after a line outage without mitigation, which starts high at ≈ 22.2 MW, and stabilizes near 21.8 MW. This indicates severe degradation in system efficiency due to the outage. The green curve is an outage with MPC-GUPFC and FRT scenario - loss History that models system response after the same outage but with MPC-GUPFC and FRT control strategy applied. The plot reveals that the loss starts at 13.2 MW, converging to 12.2 MW. This demonstrates that FRT and MPC-GUPFC significantly reduce losses compared to the unmitigated outage (blue), but not as low as the original base case (red). The results reveal that implementing FRT with the MPC-GUPFC strategies can significantly reduce the adverse effects of system faults, ensuring better power quality and lower system losses. This is essential for resilient and smart power grids.

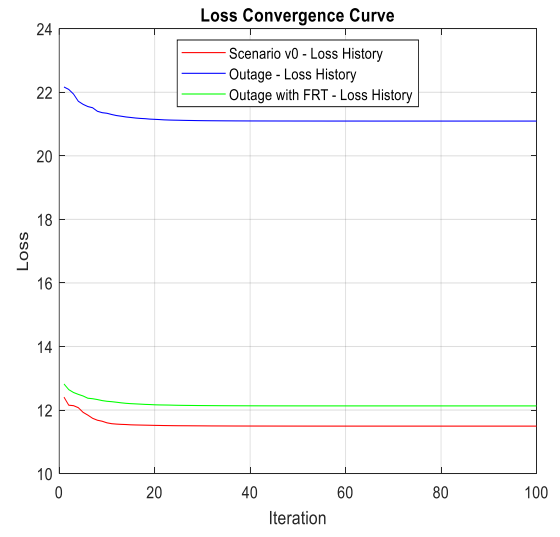


Fig. 8. MW loss convergence curve

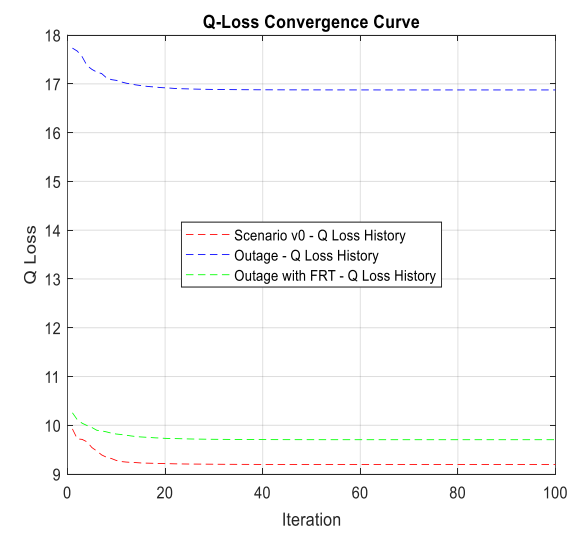
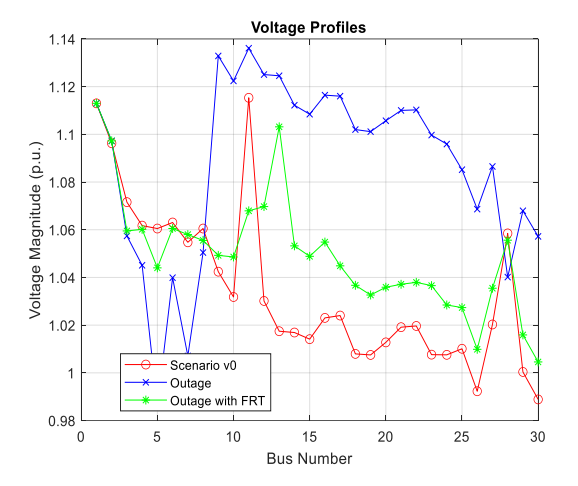


Fig. 9. MVAr loss convergence curve

Fig. 9 shows the reactive power loss (Q loss) convergence behaviour over 100 iterations for three different scenarios in the testbed. Scenario v0, Q loss history (Red solid line), represents the base system under normal conditions (no outage, no fault). It starts around 10.0 MVAr and quickly converges to about 9.3 MVAR within ~10 iterations. This is the most efficient case, exhibiting the lowest final Q loss. Outage scenario, Q loss history (Blue, dashed line), which includes a line outage without any compensating strategy. It starts at a high Q loss (~17.8 MVAr) and converges slowly to around 16.9 MVAr. This represents a heavily degraded system, showing that outage leads to increased reactive power demand and poor voltage support. Outage with FRT and GUPFC, Q loss history (Green, dash-dot line) includes the same outage but with FRT and a GUPFC mitigation strategy. It begins slightly higher than Scenario v0 but converges quickly to around 9.6 MVAr that is very close to the base case. This indicates that FRT and GUPFC effectively restore system performance, mitigating the impact of the outage. The results reveal that all three scenarios stabilize within ~20 iterations, but Scenario v0 and outage with FRT and GUPFC mitigation strategy converge significantly faster and lower than the outage-only case. The plot clearly demonstrates that FRT mechanisms and MPC-GUPFC are effective in minimizing reactive power losses during line outages. The comparative convergence trend justifies the technical value of investing in smart control infrastructure for grid reliability and stability.

A voltage profile plot across the IEEE 30-bus system under three different scenarios is presented in Fig. 10. Three scenarios are compared; the scenario v0 (Red circles) - Normal operating condition (no outage), outage (Blue crosses) - Line outage or contingency condition, and outage with FRT and MPC-GUPFC (Green stars) - Outage mitigated using FRT strategy and MPC-GUPFC.



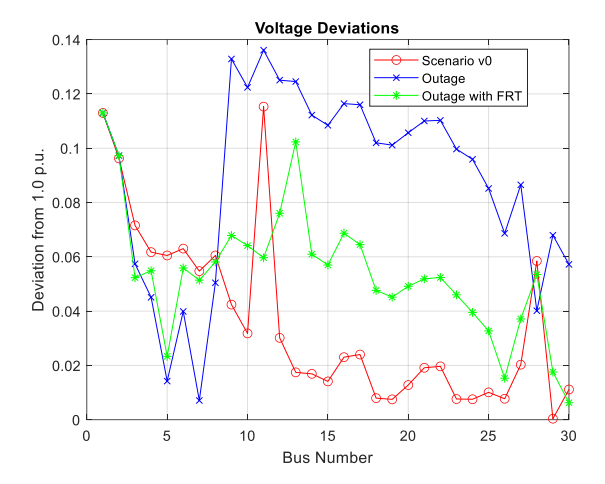


Fig. 10. Voltage profiles plots

Fig. 11. Voltage deviations plots

In the scenario v0 (Red) which is normal operation, voltage profile is well regulated, mostly between 1.00 and 1.05 p.u., which shows ideal voltage levels, indicating balanced, stable operation, which is expected behaviour with minimal fluctuation and proper voltage control. In the outage (Blue), No mitigation, many buses show elevated voltage levels, exceeding 1.05 p.u., which signifies voltage imbalance is significant, particularly between Bus 1 and Bus 15. This indicates voltage rise or drop due to the redistribution of power flow induced by the outage, which is potential voltage violation beyond acceptable limits (>1.05 p.u.). The outage mitigated with MPC-GUPFC and FRT strategies (Green), voltage profile is much smoother and closer to base case (Red). Though not perfect, most buses are maintained within acceptable bounds (~1.00 p.u. –1.08 p.u.). This demonstrates that MPC-GUPFC and FRT improve grid voltage stability under fault conditions, helping restore post-contingency performance to near-nominal levels.

Fig. 11 presents voltage deviation across all 30 buses under 3 different scenarios. Scenario v0 (Red line with circles), which is the base case (normal operation - no outage, no FRT, no MPC-GUPFC). Here, the system maintains voltage near the nominal value (1.0 pu). Outage scenario (Blue line with X markers) represents the system after a critical line outage, without any mitigation. Deviation > 0.12 pu is significant and could threaten system voltage stability, especially around buses 10 to 20. This reflects the destabilizing impact of the outage. Outage with FRT and MPC-GUPFC (Green line with stars), where FRT and MPC-GUPFC are jointly implemented to mitigate the outage's effect. It is noted that the deviation line drops closer to Scenario v0, showing much better voltage support compared to the unmitigated outage case. FRT + MPC-GUPFC (Green) pulls deviations down, nearly half the voltage deviation across most buses. It brings the worst-case deviation from ~0.136 pu (blue) to ~0.060 pu (green); and this demonstrates effective dynamic voltage control and support. The key insights of these results are outage alone degrades voltage quality significantly, integrated mitigation strategy (FRT + MPC-GUPFC) substantially restores voltage stability. Therefore, these results strongly validate the usefulness of the hybrid control approach for enhancing system resiliency during critical contingencies.

Fig.12 presents the reactive power (Q) dispatch plot that shows a comparative view of how Q is generated and consumed across different buses in the testbed under various operating conditions. Multiple curves are plotted to reflect different scenarios: baseline operation (v0), line outage without and with MPC-GUPFC and FRT adjustments. For Q generation, buses 1 to 13 are the primary generators. The green curve marked with circles represents Q generation under normal conditions (v0 – Gen), serving as a reference for system behavior without any faults. The blue curve with circles shows Q generation during a line outage without MPC-GUPFC and FRT support, revealing significant spikes at certain buses—particularly around Buses 3, 5 and 8. These spikes suggest that the system compensates for the fault by dispatching more Q at strategic locations, likely to maintain voltage stability. The red curve with circles illustrates Q generation when MPC-GUPFC and FRT mechanisms are applied during an outage. Compared to the pure outage scenario, this curve is smoother and less volatile, indicating that MPC-GUPFC and FRT support helps stabilize the system by moderating Q dispatch.

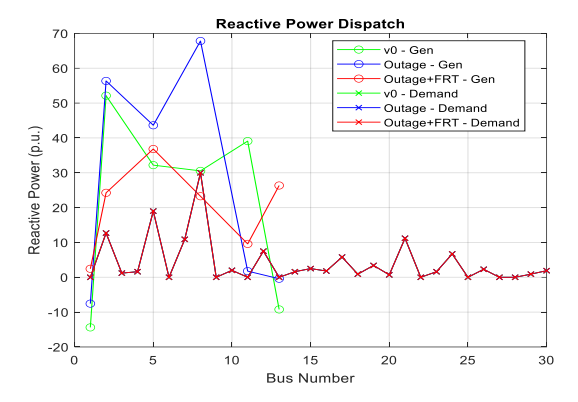


Fig. 12. The reactive power dispatch plots

For the Q demand, the red curve with stars represents Q demand under the outage with MPC-GUPFC and FRT condition. It remains consistent across all buses, suggesting that demand is unaffected by the fault or the corrective measures. Interestingly, the plot legend includes two additional curves, v0 – Demand and Outage – Demand without MPC-GUPFC and FRT mechanisms, marked by green and blue stars, respectively. However, these curves are not visible on the graph. This absence can be explained by a fundamental principle of power system operation, load balancing. In steady-state simulations, the demand at each bus is typically treated as fixed. Regardless of generator conditions or fault scenarios, the system must ensure that the load is served. As a result, the Q demand remains constant across scenarios. Because the demand does not change in response to generator behavior, the curves for v0 - Demand and Outage without MPC-GUPFC and FRT mechanisms - Demand overlap perfectly with the outage with MPC-GUPFC and FRT mechanisms - adjusted demand curve. This makes them visually indistinct or redundant, and they may have been omitted from the plot either automatically by the plotting tool or intentionally to reduce clutter. In essence, while Q generation adapts dynamically to system conditions, rising sharply during faults and stabilizing with MPC-GUPFC and FRT mechanisms, the demand remains steady. This reflects the core operational requirement of load balancing: the system must dispatch sufficient Q to meet fixed demand, regardless of disruptions or control strategies.

Fig. 13 presents a real power loss comparison plot. The scenario v0 (Red circles) represents the normal operation of the system without any fault or outage. In this scenario it is noted that only a few branches (mostly among the first 10) show noticeable real power losses (up to \sim 4.5 MW), which is typical in a stable power system.

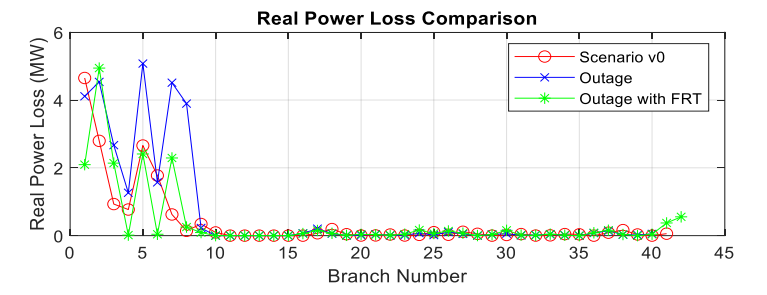


Fig. 13. Real power loss comparison plot

The outage (Blue x markers) scenario represents the system during a branch outage (fault scenario). Here, it is observed that noticeable spikes in power loss occur in branches 1 through 10, especially branch 5 and 7. This indicates the redistribution of power due to the outage that increases losses in certain lines. Some branches that had minimal losses under normal conditions now experience significant losses, pointing to stress and inefficiency in the network during the fault. The outage with MPC-GUPFC and FRT (Green stars) represents the fault scenario but with MPC-GUPFC and FRT support. In this scenario, compared to the blue curve, power losses are significantly reduced in almost all branches. Summarily, it can be stated that the green curve closely follows the red curve (normal scenario), indicating that MPC-GUPFC and FRT mechanisms mitigate the negative impacts of the outage.

Fig. 14 presents reactive power loss vs branch number plot that shows three different Scenarios: Scenario v0 (Red circles) that represents normal operation (base case), Outage (Blue crosses) that shows increased reactive power loss due to branch failure, and Outage with MPC-GUPFC with FRT (Green stars) that incorporates FRT and MPC-GUPFC to mitigate outage effects.

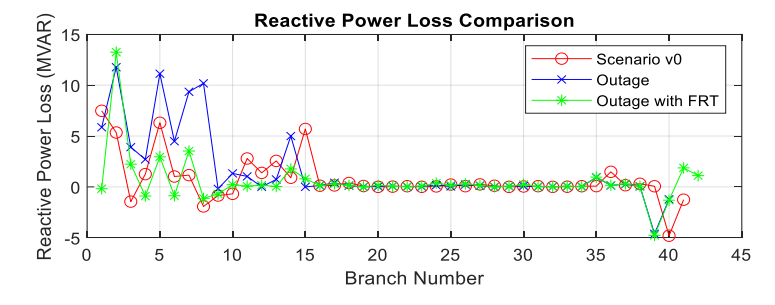


Fig. 14. Reactive power loss comparison plot

From the Fig. 14, it is observed that there is high reactive power loss in branches 1 through 10. The outage scenario (blue crosses) shows significant spikes, indicating reactive power instability. The MPC-GUPFC and FRT scenario (green stars) successfully lowers losses. A closer look at the plot reveals that there is stabilization in mid-segment branches 10 through 30, where reactive power loss declines and stabilizes across all scenarios. This suggests that branches beyond number 10 are less sensitive to failures. There are minor fluctuations in later branches (>30) that indicate small disturbances in some branches. All in all, MPC-GUPFC and FRT improve system stability, keeping losses in check. This analysis reinforces that FRT and FACTs mechanisms play a vital role in maintaining power system reliability.

4.1.4. Cost of deployment of MPC based GUPFC

In this study, the effective loading obtained from simulation was 14.03 MVAr. Upon using this value in Eq. (38), we obtained \$55,226.15. To that effect, the cost of deploying the MPC-GUPFC mechanism was \$55,226.15, reflecting its economic feasibility in reducing power losses and stabilizing the grid.

4.2. Validation of the study

Table 2 presents a comparison table that highlights key differences between our study and recent and relevant literature, focusing on key aspects such as objectives, methods, devices used, control strategies, and unique contributions. Table 2 reveals that the study fills a significant gap in literature by co-applying FRT and MPC logic within a GUPFC structure, a configuration rarely explored in previous works, which often relied on linear or static FACTS models

Table 2. Comparative Analysis of recent work versus present study

Ref	Objective	Method used	FACTS device	Control strategy	FRT	ORPD integrated	Gaps identified
[5]	Minimize voltage deviation under renewables	Hybrid Whale-BAT algorithm	GUPFC	Static Control	No	Yes	No dynamic control under faults
[6]	Improve voltage during faults in wind farms	Model Predictive Control (MPC)	SMES	MPC-based control	Yes	No	No ORPD or FACTS device coordination
[7]	Low-voltage ride- through in inverters	Predictive control	Inverter system	MPC	Yes	No	Lacks network-level optimization
[8]	ORPD optimization on IEEE 30-bus	Hybrid multi- objective algorithm	None	Heuristic	No	Yes	No FACTS, no fault dynamics
Present Study	Robust ORPD under line outage	HPSOBAT + Sensitivity Analysis	GUPFC	MPC + FRT	Yes	Yes	_

5. Conclusion

This study has presented a robust and integrated framework for enhancing Optimal Reactive Power Dispatch in electric power systems under critical contingency conditions through the combined application of a Model Predictive Control (MPC) based Generalized Unified Power Flow Controller (GUPFC) and a Fault Ride-Through (FRT) enhancement strategy. By employing a Performance Index based contingency analysis, the most critical transmission line outage was effectively identified and mitigated, thereby reinforcing grid resilience under dynamic operating conditions. The proposed scheme demonstrated its capability to substantially improve voltage stability and reduce active power losses during post-contingency scenarios. Through predictive control and flexible FACTS-based interventions, the framework ensured that system parameters were maintained within permissible bounds while supporting secure and efficient operation. The incorporation of the HPSOBAT optimization algorithm further enabled adaptive tuning of controller parameters, guaranteeing both constraint satisfaction and operational efficiency.

Overall, the integration of FRT with an MPC-controlled GUPFC, optimized via HPSOBAT, provides a scalable and effective solution for addressing both transient stability and reactive power management in modern power networks. Future research may extend this work by applying the framework to multi-objective dynamic OPF problems, particularly in renewable-rich or meshed transmission systems, where the challenges of uncertainty and variability are more pronounced.

Acknowledgment

The authors of this paper recognize with gratitude the Department of Electrical & Electronics Engineering of the University of Lagos, Lagos, Nigeria for the provision of essential backing for the materialization of this study

References

- [1] M. H. Ali, A.M.A. Soliman, M. Abdeen, T. Kandil, A.Y. Abdelaziz, and A. El-Shahat, "A novel stochastic optimizer solving optimal reactive power dispatch problem considering renewable energy resources", Energies 2023, 16, 1562. https://doi.org/10.3390/en16041562.
- [2] I.H. Shanono, A. Muhammad, N.R.H. Abdullah, H. Daniyal, and M.C. Tiong, "Optimal reactive power dispatch: a bibliometric analysis", Journal of Electrical Systems and Inf Technol", vol. 8, no. 1, pp. 1-23, 2021, https://doi.org/10.1186/s43067-020-00024-5.
- [3] I. Marouani, T. Guesmi, H.H. Abdallah, and A. Ouali, "Optimal reactive power dispatch considering FACTS devices", Leonardo Journal of Sciences, vol. 10, no. 18, pp. 97-114, 2011.
- [4] K. H. Reddy, P.R. Reddy, and V. Ganesh, "Optimal allocation of FACTS devices using kinetic gas molecular optimization and grey wolf optimization for improving voltage stability", Journal of Mechanics of Continua and Mathematical Sciences, vol. 15, no. 4, pp. 66-88, 2020, https://doi.org/10.26782/jmcms.2020.04.00007.
- [5] K. K. V. Kavuturu, K.N.V. Sai Tejaswi, and V. Janamala, "Performance and security enhancement using generalized optimal unified

- power flow controller under contingency conditions and renewable energy penetrations", Journal of Electrical Systems and Inf Technol., vol. 9, no. 18, pp. 1-24, 2022, https://doi.org/10.1186/s43067-022-00057-y.
- [6] S. M. Abdelkader, E.F. Morgan, T.F. Megahed, W. Rohouma, and O. Abdel-Rahim, "A model predictive control strategy for enhancing fault ride through in PMSG wind turbines using SMES and improved GSC control", Frontiers in Energy Research, vol. 11-2023, pp. 1-12, 2023, https://doi.org/10.3389/fenrg.2023.1277954.
- [7] J. Yuan, Y. Chen, N. Chen, Y. Zhang, and Y. Lin, "Research on low-voltage ride through control based on model predictive control", J. Eng., 13, pp. 2114–2118, 2017, https://doi.org/10.1049/joe.2017.0703.
- [8] S. A. Adegoke, Y. Sun, and Z. Wang, "A mini review on optimal reactive power dispatch incorporating renewable energy sources and flexible alternating current transmission system", Electr. Eng., 106, pp. 3961-3982, 2024, https://doi.org/10.1007/s00202-023-02199-2.
- [9] D. Das, Electrical Power Systems, New Age International (P) Ltd, New-Delhi. India, 2006.
- [10] J. J. Grainger, and W.D. Stevenson, Jr., Power System Analysis, Published by McGraw-Hill, Inc., Singapore, 1994.
- [11] J. A. Wood, B. F. Wollenberg, and G.B. Sheble, Power Generation, Operation, and Control, Third Edition, John Wiley & Sons, Inc., New York, 2014.
- [12] P. Kundur, Power system stability and control, Second Edition, John Wiley & Sons, Inc., New York, 1994.
- [13] X. Zhang, E. Handschin, and M. Yao, "Modeling of the generalized unified power flow controller (GUPFC) in a nonlinear interior point OPF", IEEE Transactions on Power Systems, vol. 16, no. 3, pp. 367-373, 2001, https://doi.org/10.1109/59.932270.
- [14] R. R. Duvvuru, B. V. Prasanth, and V. Ganesh, "Performance of generalized unified power flow controller in transmission system" International Journal of Renewable Energy Technology, vol. 9, no. 1/2, pp. 108-117, 2018, https://doi.org/10.1504/IJRET.2018.090108.
- [15] K. K. V. Kavuturu, and P. V. R. L. Narasimham, "Optimal parameters of OUPFC and GUPFC under renewable energy power variation using Cuckoo search algorithm variants", J. Electr. Eng. Technol., vol. 15, pp. 2079–2098, 2020, https://doi.org/10.1007/s42835-020-00501-x.
- [16] M. V. Rao, C. V. Suresh, and S. Sivanagaraju, "Generalized unified power flow controller for optimal reactive power dispatch by considering practical constraints", Indian Journal of Science & Technology, vol. 10, no. 5, pp. 1-7, 2017, https://doi.org/10.17485/ijst/2017/v10i5/102937.
- [17] C. V. Suresh, and S. Sivangaraju, "Multi-objective optimal reactive power dispatch to maximize power system social welfare in the presence of generalized unified power flow controller", Archives of Electrical Engineering, vol. 64, no. 3, pp. 405-426, 2015, https://doi.org/10.2478/aee-2015-0032.
- [18] K. R. Padiyar, and A. M. Kulkarni, "Control design and simulation of unified power flow controller", IEEE Trans. Power Delivery, vol. 13, no. 4, pp. 1348–1354, 1998, https://doi.org/10.1109/61.714962.
- [19] J. Sun, H. Zheng, C. L. DeMarco, and Y. Chai, "Energy function-based model predictive control with UPFCs for relieving power system dynamic current violation", IEEE Transactions on Smart Grid, vol. 7, no. 6, pp. 2933-2942, 2016, https://doi.org/10.1109/TSG.2016.2582878.
- [20] R. Sadiq, U. Naeem, and M. Shahzad, "Power system stabilization using unified power flow controller and model predictive control", 2019 International Symposium on Recent Advances in Electrical Engineering (RAEE), Islamabad, Pakistan, pp. 1-6, 2019, https://doi.org/10.1109/RAEE.2019.8887022.
- [21] A. N. B. Alsammak, and H. Adnan, "Power quality improvement using fuzzy logic controller based unified power flow controller", Indonesian Journal of Electrical Engineering and Computer Science, vol. 21, no. 1, pp. 1-9, 2021, https://doi.org/10.11591/ijeecs.v21.i1.pp1-9.
- [22] S. Ghaedi, S. Abazari, and G. A. Markadeh, "Transient stability improvement of power system with UPFC control by using transient energy function and sliding mode observer based on locally measurable information", Measurement, 183, 109842, 2021, https://doi.org/10.1016/j.measurement.2021.109842.
- [23] S. Tiwari, R. Naresh, and R. Jha, "Neural network predictive control of UPFC for improving transient stability performance of power system", Applied Soft Computing, vol. 11, no. 8, pp. 4581-4590, 2011, https://doi.org/10.1016/j.asoc.2011.08.003.
- [24] L. H. Hassan, M. Moghavvemi, H. A. F. Almurib, and O. Steinmayer, "Application of genetic algorithm in optimization of unified power flow controller parameters and its location in the power system network", International Journal of Electrical Power & Energy Systems, 46, pp. 89-97, 2013, https://doi.org/10.1016/j.ijepes.2012.10.011.
- [25] P. M. S. Carvalho, P. F. Correia and L. A. F. M. Ferreira, "distributed reactive power generation control for voltage rise mitigation in distribution networks," IEEE Transactions on Power Systems, vol. 23, no. 2, pp. 766-772, May 2008, https://doi.org/10.1109/TPWRS.2008.919203.
- [26] S. Mirza and A. Hussain, "New Approaches in finite control model predictive control for grid-connected Photovoltaic inverters: State of the Art", Solar, vol. 4, no. 3, pp. 491-508, 2024, https://doi.org/10.3390/solar4030023.
- [27] B. Bhattacharyya, V. K. Gupta, and S. Kumar, "UPFC with series and shunt FACTS controllers for the economic operation of a power system", Ain Shams Engineering Journal, vol. 5, no. 3, pp. 775-787, 2014, http://dx.doi.org/10.1016/j.asej.2014.03.013.
- [28] S. S. Padaiyatchi, and S. Jaya, "Hybrid Bat optimization algorithm applied to optimal reactive power dispatch problems", International Journal of Electrical and Electronics Engineering, vol. 9, no. 1, pp. 1-9, 2022, https://doi.org/10.14445/23488379/IJEEE-V9I1P101.
- [29] M. Ellahi, G. Abbas, G. B. Satrya, M. R. Usman, and J. Gu, "A modified hybrid particle swarm optimization with bat algorithm parameter inspired acceleration coefficients for solving eco-friendly and economic dispatch problems", IEEE Access, 9, pp. 82169-82187, 2021, https://doi.org/10.1109/ACCESS.2021.3085819.
- [30] S. Mugemanyi, Z. Qu, F.X. Rugema, Y. Dong, C. Bananeza, and L. Wang, "Optimal reactive power dispatch using chaotic bat algorithm", IEEE Access, 8, pp. 65830-65867, 2020, https://doi.org/10.1109/ACCESS.2020.2982988
- [31] S.O. Adetona, M. John, and S. Umar, "Optimal reactive power dispatch using improved chaotic PSO algorithm with the wingbeat frequency", Acta Marisiensis. Seria Technologica, vol. 19 (XXXVI), no. 2, pp. 20-29, 2022, https://doi.org/10.2478/amset-2022-0013
- [32] MathWorks, Inc., 2024, MATLAB (Version R2024b) [Software][Online]. Available: https://www.mathworks.com
- [33] R. D. Zimmerman, C. E. Murillo-Sánchez, and R. J. Thomas, "MATPOWER: Steady-state operations, planning, and analysis tools for power systems research and education", IEEE Trans. on Power Systems, vol. 26, no. 1, pp. 12-19, 2011, https://doi.org/10.1109/TPWRS.2010.2051168.
- [34] University of Washington, "Power systems test case archive", 1999 [Online]. Available: https://labs.ece.uw.edu/pstca/pf30/pg tca30bus.htm.